Hindawi
Journal of Nanomaterials
Volume 2017, Article ID 5264910, 11 pages
https://doi.org/10.1155/2017/5264910

Research Article

Performance of $NiFe_2O_4$-SiO_2-TiO_2 Magnetic Photocatalyst for the Effective Photocatalytic Reduction of Cr(VI) in Aqueous Solutions

Mike O. Ojemaye,[1,2] Omobola O. Okoh,[1,2] and Anthony I. Okoh[2]

[1]*Department of Pure and Applied Chemistry, University of Fort Hare, Alice 5700, South Africa*
[2]*SAMRC, Microbial Water Quality Monitoring Centre, University of Fort Hare, Alice, South Africa*

Correspondence should be addressed to Mike O. Ojemaye; mikeojemaye@gmail.com

Received 2 November 2016; Revised 15 December 2016; Accepted 25 December 2016; Published 16 January 2017

Academic Editor: William Yu

Investigation into the reduction of Cr(VI) in aqueous solution was carried out through some batch photocatalytic studies. The photocatalysts used were silica coated nickel ferrite nanoparticles ($NiFe_2O_4$-SiO_2), nickel ferrite titanium dioxide ($NiFe_2O_4$-TiO_2), nickel ferrite silica titanium dioxide ($NiFe_2O_4$-SiO_2-TiO_2), and titanium dioxide (TiO_2). The characterization of the materials prepared via stepwise synthesis using coprecipitation and sol-gel methods were carried out with the aid of X-ray diffraction (XRD), transmission electron microscopy (TEM), scanning electron microscopy (SEM), Fourier transform infrared (FTIR) spectroscopy, thermal gravimetric analysis (TGA), and vibrating sample magnetometry (VSM). The reduction efficiency was studied as a function of pH, photocatalyst dose, and contact time. The effects of silica interlayer between the magnetic photocatalyst materials reveal that reduction efficiency of $NiFe_2O_4$-SiO_2-TiO_2 towards Cr(VI) was higher than that of $NiFe_2O_4$-TiO_2. However, TiO_2 was observed to have the highest reduction efficiency at all batch photocatalytic experiments. Kinetics study shows that photocatalytic reduction of Cr(VI) obeyed Langmuir-Hinshelwood model and first-order rate kinetics. Regenerability study also suggested that the photocatalyst materials can be reused.

1. Introduction

Heavy metal pollution has become one of the most serious environmental problems today. Their toxicity and persistence have made their treatment and remediation from the environment pertinent. Wastewater containing hazardous metals generated by industries is continually discharged into the environment especially fresh water resources causing severe health risks. These toxic metals unlike organic contaminants are not biodegradable and when accumulated in the body cause severe damage and sometimes death [1]. Chromium is one of the most frequently found metals in the environment because of its usage in major industries such as metal plating, petrochemicals, mining, fertilizer, tanneries, batteries, pesticides, and paper industries [2, 3] but it is a source of concern and risk to human because of its toxicity, cancer causing tendencies, and free movement in water. Different valence forms of chromium are known but in water bodies Cr(VI) and Cr(III) forms are most common. The valence state of chromium determines its behavior. Whereas Cr(III) is immobile and nontoxic, Cr(VI) is highly toxic, cancerous, and mobile [4]. In the past, extensive studies on various techniques of Cr(VI) removal from wastewater have been reported. These include coagulation [5], membrane separation and ion exchange [6], solvent extraction and electrochemical destruction [7], and ozonation and aerobic/anaerobic microbial degradation [8, 9]. Despite the availability of these techniques, limitations encountered with these technologies such as cost, high energy requirement, and large use of reducing agents [10] are noticeable drawbacks. Also, semiconductor photocatalysts such as titanium dioxide (TiO_2), zinc oxide (ZnO), cadmium sulfide (CdS), tin oxide (SnO), and tungsten oxide (WO_3) have been employed for the reduction of Cr(VI) in wastewater. Although titanium

dioxide photocatalysts have been shown to be the most efficient due to their superior oxidation and reduction capability, nontoxicity, low cost of preparation, and chemical and biological inertness [11–14], however, problems such as difficulty of separation and recycling of photocatalyst materials from wastewater are encountered. Efforts made to overcome these problems include supporting titania on silica, glass, zeolite, and fibre glass [7, 15–19]. Also, magnetic nanoparticles have been reported as supports to aid the recycling and ease the separation of titanium photocatalyst but all these reduce the photocatalytic activity of titanium dioxide to an extremely low point due to the immobility of the photocatalyst and low mass transfer rate. To address these problems, the use of magnetic photocatalysts containing various molar ratios of magnetic nanoparticles and TiO_2 as well as the use of an inert layer such as silica between titania and magnetic nanoparticles allows for easy separation with the aid of an external magnet and recyclability while maintaining the photocatalytic properties of titania [20, 21].

In this study, we report on the effectiveness of magnetic titanium dioxide nanocomposite with silica interlayer ($NiFe_2O_4$-SiO_2-TiO_2) to photocatalytically reduce Cr(VI) in aqueous solution. In addition, $NiFe_2O_4$-TiO_2 nanocomposite, TiO_2 photocatalyst, and $NiFe_2O_4$-SiO_2 were synthesized and assessed for Cr(VI) reduction. Furthermore, the photocatalytic activities of the photocatalyst composites were compared to determine if the introduction of silica interlayer enhanced the reduction of Cr(VI) from aqueous solution. The nanocomposites were prepared by stepwise methods starting with coprecipitation followed by the hydrolysis of SiO_2 and TiO_2 for $NiFe_2O_4$-SiO_2-TiO_2 and hydrolysis of only TiO_2 for $NiFe_2O_4$-TiO_2. Most published works are on the use of titanium dioxide-carbon nanocomposite and titanium dioxide photocatalysts on the reduction of Cr(VI) in aqueous solutions [4, 10] and to the best of our knowledge there has been no report on the use and comparison of the photocatalytic performance of $NiFe_2O_4$-SiO_2-TiO_2 and $NiFe_2O_4$-TiO_2 nanocomposites for the reduction of toxic Cr(VI) from aqueous solution. The optimum conditions necessary for Cr(VI) reduction were also investigated using batch photocatalytic adsorption processes involving the effect of pH, contact time, and catalyst dose. Regenerability studies using the spent photocatalyst materials were also carried out on the reduction of Cr(VI) in aqueous solution to determine their reusability.

2. Experimental

2.1. Chemicals. All Chemicals used were of analytical grade. Titanium(IV) isopropoxide 97%, titanium tetrachloride, and diethoxyl dimethylsilane were purchased from Sigma Aldrich, Gauteng, South Africa, while $NiCl_2{\cdot}6H_2O$, $FeCl_3{\cdot}6H_2O$, potassium dichromate salt, NaOH, HCl, and absolute ethanol (HPLC grade) were purchased from Merck Chemicals Ltd., South Africa. Deionized water was used for the experiment.

2.2. Preparation of Nickel Ferrite Nanoparticles. Nickel ferrite nanoparticles were prepared by the coprecipitation method [22]. Molar solutions of $FeCl_3{\cdot}6H_2O$ and $NiCl_2{\cdot}6H_2O$ in ratio 2 : 1 were prepared and 30 cm^3 of each solution was mixed and stirred under nitrogen for 30 min. NaOH of 10 mol dm^{-3} was slowly added to the reacting mixture until the pH of the mixture attained 11. The temperature of the reaction mixture was taken up to 80°C and the mixture was allowed to stir for another 90 min under an inert nitrogen condition. The large amount of precipitate generated was filtered, washed twice with ethanol and severally with deionized water with repeated centrifugation at 4000 rpm for 10 min until the pH was about 7, and dried overnight at 80°C.

2.3. Preparation of $NiFe_2O_4$-SiO_2. SiO_2 was used to coat the surface of $NiFe_2O_4$ using the method of Laohhasurayotin et al. (2012) with slight modification. 300 mg of $NiFe_2O_4$ nanoparticle placed in a 250 cm^3 round bottom flask was dispersed in 25 cm^3 solution of ethanol using a water bath ultrasonicator for 1 h. Diethoxydimethylsilane (0.7 cm^3) and 30% NH_3 (0.6 cm^3) were both added gradually while stirring in the sonicator bath for 3 h at 25°C. The resulting precipitate was collected by centrifugation after washing severally with water and dried overnight at 80°C followed by calcination at 450°C for 2 h [23].

2.4. Preparation of Titanium Dioxide Photocatalyst. In 200 cm^3 of deionized water placed in an ice bath with vigorous stirring, 11 cm^3 of titanium tetrachloride was added dropwise. The resulting solution was allowed to undergo hydrolysis by heating at 80°C for 30 min. Sodium hydroxide solution was used to adjust the pH to around 8-9. The white precipitate formed was washed thoroughly with deionized water to remove excess chloride ions and was collected via centrifugation and dried in an oven at 70°C overnight. The white powder obtained after oven drying was calcined at 450°C for 2 h.

2.5. Preparation of Nanocomposite Samples ($NiFe_2O_4$-SiO_2-TiO_2 and $NiFe_2O_4$-TiO_2). Nanocomposites were prepared using the sol-gel method. 200 mg of $NiFe_2O_4$-SiO_2 nanoparticles in a round bottom flask was dispersed in 25 cm^3 ethanol and sonicated in an ultrasonic water bath apparatus for 60 min at room temperature. 0.1 M HCl solution was used to adjust the pH of the suspension to 4.0. Titanium(IV) isopropoxide (0.2 cm^3) in 10 cm^3 ethanol was slowly added into the suspension above and ultrasonicated while stirring for 4 h at 80°C to ensure uniformity of mixture. The precipitate obtained was filtered and washed with ethanol and then deionized water until the pH was about 7.0. The particles were left to age at room temperature for 1 h and then dried overnight at 80°C and later calcined at 450°C for 2 h. For the synthesis of $NiFe_2O_4$-TiO_2, the same method was followed except that $NiFe_2O_4$ was used [23].

2.6. Characterization. Characterization of the synthesized materials was done using XRD to determine the crystallite size, crystalline phase, and purity of the photocatalysts. This was recorded on a Bruker D8 Advanced, equipped with a proportional counter using Cu Kα radiation (λ = 1.5405 Å,

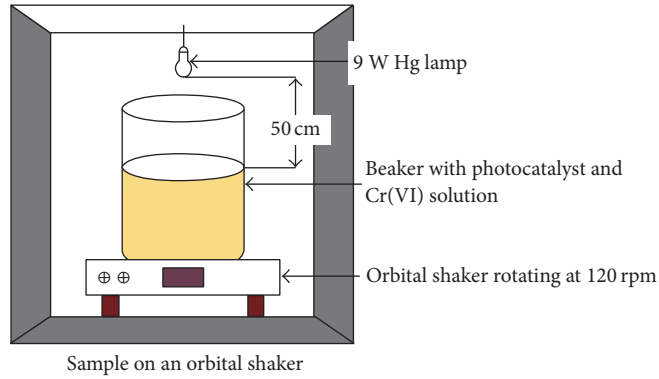

Figure 1: Photocatalytic setup for the reduction of Cr(VI) using 9 W Hg lamp.

nickel filter). Scanning electron microscope (SEM) images were recorded using JOEL JSM-6390 LVSEM. Transmission electron microscope (TEM) was done to determine the shape and confirm the particle size of the material. Fourier transform infrared (FTIR) spectroscopy was used to observe the vibrations of the composite samples. Perkin-Elmer Universal ATR sampling accessory spectrum 100 FTIR spectrometer was used to collect the IR spectra of the samples. Thermal gravimetric analyzer was used to determine the purity and thermal stability of the materials; thermogravimetric analysis (TGA) was performed using a Perkin-Elmer TGA 4000 analyzer. The magnetic properties of the photocatalyst composites were quantified using a cryogen free physical measurement vibrating sample magnetometer (VSM) at a temperature range of 1.8 to 310 K with a magnetic system of 14 tesla.

2.7. Photocatalytic Experiment. To evaluate the photocatalytic capability of the prepared photocatalyst against the reduction of Cr(VI) in aqueous solution, a photocatalytic reactor made of a 500 cm^3 glass beaker, an orbital shaker, and a mercury (Hg) lamp of a wavelength of 254 nm were employed (Figure 1). Typically, 10 mg/L of potassium dichromate solution was used. Before UV illumination, 200 mg of photocatalyst was suspended in 100 cm^3 potassium dichromate solution in a 500 cm^3 beaker covered with a parafilm to prevent evaporation and subjected to agitation at 120 rpm for 30 minutes in the dark to ensure the attainment of equilibrium of adsorption or desorption between Cr(VI), photocatalyst, and water. This solution was then irradiated with 9 W Hg lamp at room temperature. The mixture was centrifuged and filtered through a 0.22 micrometer membrane filter after 300 min and the final concentration of Cr(VI) was determined using a UV-Vis spectrophotometer at 350 nm. The effect of pH, time, and catalyst dose was studied for each photocatalyst to determine the optimum conditions necessary for photocatalysis. The photocatalytic reduction efficiency (RE) was calculated using

$$\mathrm{RE} = \frac{C_o - \mathrm{C}}{C_o} \times 100\%, \quad (1)$$

where C_o is the initial concentration of Cr(VI) solution and C is the absorbance of Cr(VI) solution at the irradiation time (t).

2.8. Regenerability Study. In a 50 cm^3 beaker, 50 mg of spent photocatalyst materials was agitated with 25 cm^3 of 0.1 N NaOH for 1 h. The titanium dioxide photocatalyst was collected by filtration and the magnetic photocatalyst composites were separated from the solution by an external magnet. The materials were dried in an oven at 105°C overnight and reused two more times for the photocatalytic reduction of Cr(VI) in aqueous solution. The % reduction of Cr(VI) after 3 runs was calculated using (1).

3. Results and Discussion

The synthesized photocatalysts were characterized using different techniques to confirm that they will be effective for the reduction of Cr(VI) in aqueous solution. The effect of silica interlayer on the magnetic photocatalyst for the reduction of Cr(VI) was investigated and compared with that of TiO_2 and bare magnetic titanium dioxide composite sample by means of some batch photocatalytic experiments.

3.1. Characterization of Photocatalysts. X-ray diffraction patterns of $NiFe_2O_4$-SiO_2, $NiFe_2O_4$-TiO_2, and $NiFe_2O_4$-SiO_2-TiO_2as well as that of titanium dioxide photocatalyst are shown in Figure 2. The most intense diffraction peaks and the average crystallite size spacing D observed experimentally were compared and indexed using JCPDS, Card nos. 10-0325 and 021-1272 for $NiFe_2O_4$ and TiO_2 in the spinel and anatase phase, respectively. From Figure 2, it is observed that sharp and intense peaks for $NiFe_2O_4$-SiO_2 observed at 2θ values of 30.5, 35.5, 44.0, 54.0, 63.0, and 75.0 with corresponding planes of (220), (311), (400), (422), (440), (533), and (511) indicate that $NiFe_2O_4$ is the main phase and shows the crystalline nature of the sample [20]; the SiO_2 peak is not observed because of its amorphous nature while the peaks observed at 2θ values for TiO_2 photocatalyst of 25.5, 48, 55, and 71 with corresponding planes of (101), (202), (105), and (116) alongside the peaks and planes of $NiFe_2O_4$ in the XRD pattern of $NiFe_2O_4$-SiO_2-TiO_2 and $NiFe_2O_4$-TiO_2 composite samples show the successful incorporation of $NiFe_2O_4$-SiO_2 and $NiFe_2O_4$, respectively, in the composite catalysts [24, 25]. The crystallite sizes of $NiFe_2O_4$, $NiFe_2O_4$-TiO_2, $NiFe_2O_4$-SiO_2-TiO_2, and TiO_2 obtained using Scherrer formula with (311) and (101) diffraction peaks for $NiFe_2O_4$

Table 1: Composition and crystallite size of $NiFe_2O_4$-SiO_2 and photocatalysts.

Samples	Crystallite size of $NiFe_2O_4$ (nm)	Crystallite size of TiO_2 (nm)	Composition of TiO_2 (%)
$NiFe_2O_4$-SiO_2	29.90	—	—
$NiFe_2O_4$-TiO_2	29.67	22.88	68.13
$NiFe_2O_4$-SiO_2-TiO_2	29.49	20.07	63.60
TiO_2	—	18.62	100.0

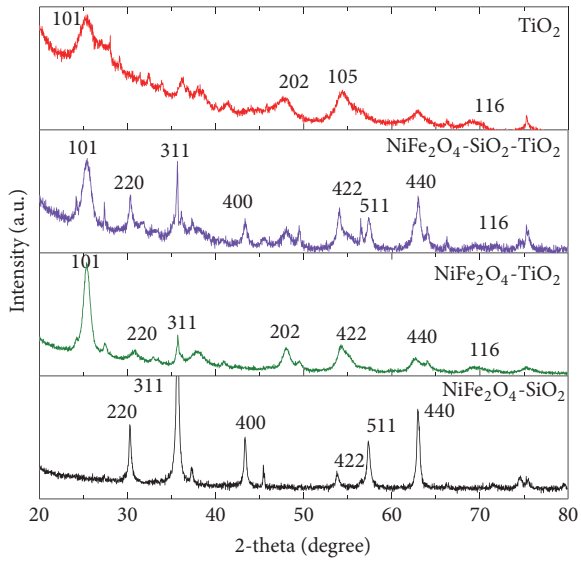

Figure 2: XRD pattern of $NiFe_2O_4$-SiO_2 nanoparticle, $NiFe_2O_4$-SiO_2-TiO_2, $NiFe_2O_4$-TiO_2, and TiO_2 photocatalysts.

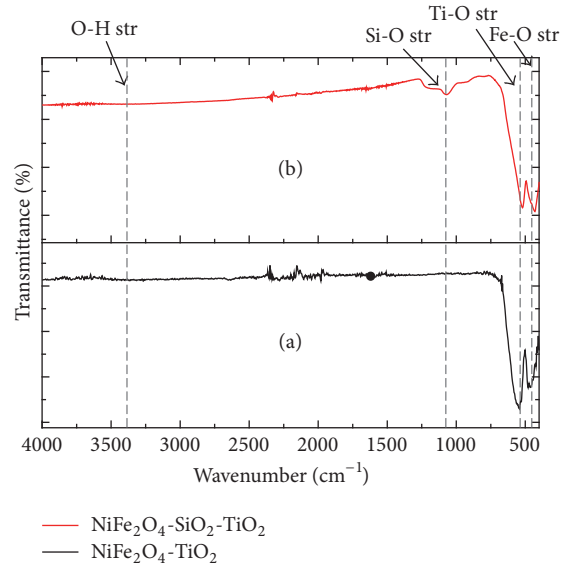

Figure 3: FTIR spectra of (a) $NiFe_2O_4$-TiO_2 and (b) $NiFe_2O_4$-SiO_2-TiO_2 photocatalysts.

and TiO_2, respectively, are listed in Table 1. The analysis shows that as the composite sample is formed, the crystallite size of $NiFe_2O_4$ decreases which is evident in the weakening of the line intensities of $NiFe_2O_4$ and that nickel ferrite possesses a cubic spinel structure while the titanium dioxide exists in the anatase crystalline phase which is in agreement with recently published report [26].

Figure 3 shows the FTIR spectra of (a) $NiFe_2O_4$-TiO_2 and (b) $NiFe_2O_4$-SiO_2-TiO_2. The absorption bands between 3354.08 cm^{-1} and 3328.40 cm^{-1} in both spectra are ascribed to the stretching mode of the hydroxyl groups on the surface of the photocatalysts. This is important as it enhances the photocatalytic activity of $TiO_2$by providing higher capacity for the adsorption of oxygen [26]. Bands observed at 456.84 cm^{-1} and 430.33 cm^{-1} for $NiFe_2O_4$-TiO_2 and $NiFe_2O_4$-SiO_2-TiO_2, respectively, are assigned to the stretching vibrations of Ti-O in anatase TiO_2 as described by Li et al. [27]. However, a band observed at 1068.69 cm^{-1} corresponding to the Si-O-Si stretching vibration in the FTIR spectra of $NiFe_2O_4$-SiO_2-TiO_2 confirmed the introduction of SiO_2 in the composite sample and this band was found to be absent in the spectra of $NiFe_2O_4$-TiO_2photocatalyst. This SiO_2 phase is however not observed in the XRD pattern and the absence is due to the fact that SiO_2 occurs in the amorphous phase and this observation has been reported in recently published results [20, 26, 28, 29]. This therefore confirms the successful synthesis of the composite photocatalyst materials.

SEM was used to investigate the structural morphology of the photocatalysts and $NiFe_2O_4$-SiO_2 nanoparticles. Figure 4 shows the SEM images of (a) $NiFe_2O_4$-SiO_2, (b) TiO_2, (c) $NiFe_2O_4$-TiO_2, and (d) $NiFe_2O_4$-SiO_2-TiO_2 at the same magnification. It was observed that spherical nanoparticles were exclusively obtained. However, high degree of agglomeration and different surface morphologies was observed in Figure 4(a) for the $NiFe_2O_4$-SiO_2. This may be due to the magnetic attraction between nickel ferrite and silica layers. Figures 4(c) and 4(d) show that the nucleation of $NiFe_2O_4$-TiO_2 and $NiFe_2O_4$-SiO_2-TiO_2 is heterogeneous with high degree of roughness on the surface; this effect is not observed in the pristine or pure photocatalyst (TiO_2) (Figure 4(b)) [26]. Figure 4(b) indicates that spherical shaped and few TiO_2 aggregate nanoparticles resulting from the hydrolysis of titanium dioxide precursors were obtained. This same observation was reported in a study by Yang and Zeng [30].

Images collected on TEM were used to observe the structure, size, and distribution of the materials produced. Figure 5(a) shows the TEM micrograph of the $NiFe_2O_4$-SiO_2 nanoparticles with an average size of 33.80 nm. From the graph, it can be seen that thin silica layers were used to coat the $NiFe_2O_4$ nanoparticles. The TEM micrograph

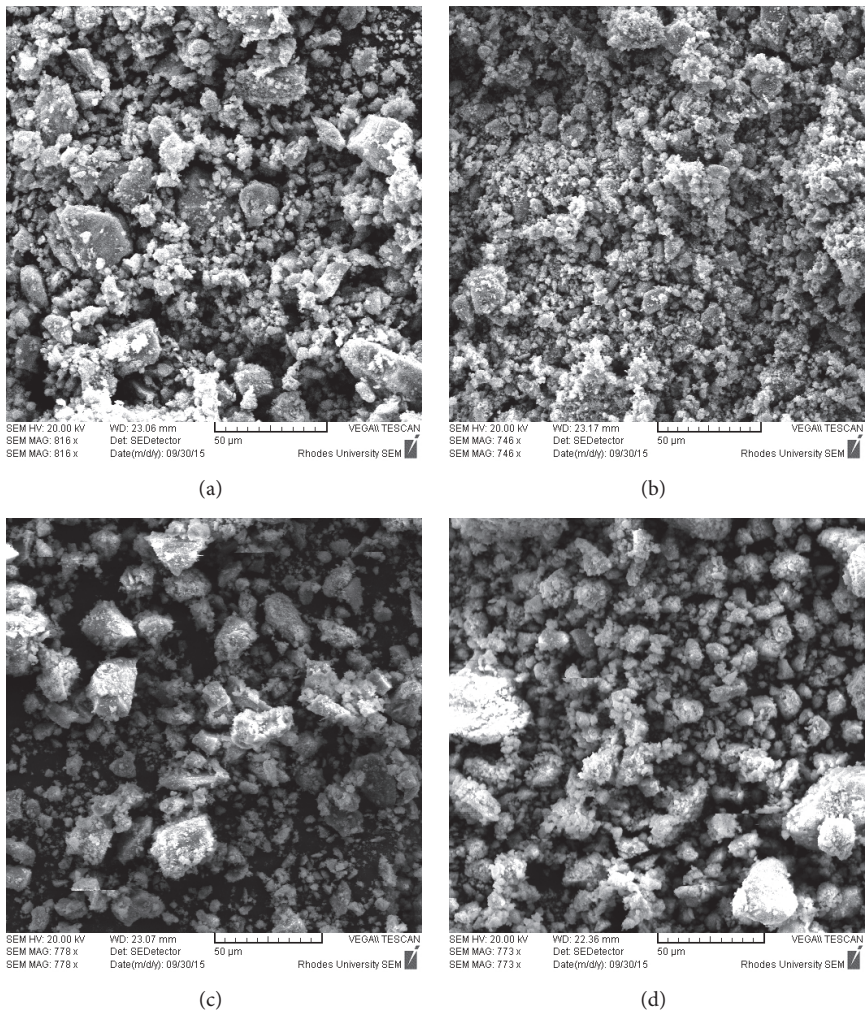

Figure 4: SEM images of (a) $NiFe_2O_4$-SiO_2, (b) TiO_2, (c) $NiFe_2O_4$-TiO_2, and (d) $NiFe_2O_4$-SiO_2-TiO_2 at the same magnification.

of $NiFe_2O_4$-TiO_2 (Figure 5(b)) shows a relatively rough spherical shaped particle. The TEM image observed at Figure 5(c) for $NiFe_2O_4$-SiO_2-TiO_2 showed similar pattern as that obtained in Figure 5(b) except that the silica layer was seen in between $NiFe_2O_4$ and TiO_2 as shown in Figure 5(c) inset; similar results have been reported in literature confirming the successful synthesis of nanoparticles and photocatalyst composites [21, 23, 26, 31, 32]. Also Figure 5(d) shows the TEM image of TiO_2 photocatalyst, the image shows that the synthesized TiO_2 photocatalyst consisted mainly of elementary particles of size ranging from 15 to 26 nm which is consistent with the results obtained from the XRD analysis (Table 1).

The thermographs of the $NiFe_2O_4$-SiO_2 and photocatalyst materials are given in Figure 6. $NiFe_2O_4$-SiO_2 is more stable than the photocatalyst materials at all temperatures. The loss of weight observed between 20 and 200°C for the photocatalyst materials in the thermograph is due to the removal of OH and H_2O indicating the presence of water molecules as also observed in their FTIR spectra [32]. However, above 200°C, the photocatalyst composites did not show any loss of weight; this confirms the stability of the materials even at higher temperatures suggesting that the presence of magnetic nanoparticles improved the stability of TiO_2. Weight loss above 200°C for TiO_2 shows that titanium dioxide can be unstable at higher temperatures.

Figure 7 shows the magnetization curves of the silica coated $NiFe_2O_4$ nanoparticles and the magnetic photocatalyst composites. It can be observed that the saturation magnetization value of the silica coated $NiFe_2O_4$ is much higher than the magnetic titanium dioxide photocatalyst; this is as a result of the nonmagnetic character of TiO_2 present in the composite samples which decreases the magnetization value of the $NiFe_2O_4$ in the composite. Although magnetic photocatalyst with silica interlayer ($NiFe_2O_4$-SiO_2-TiO_2) was observed to have a slightly higher saturation magnetization value than the $NiFe_2O_4$-TiO_2, this may be due to the presence of the SiO_2 on the $NiFe_2O_4$ which reduces the influence of the TiO_2 on the magnetic nanoparticles. This result therefore indicates that both magnetic photocatalyst composite materials exhibit supermagnetic properties at room temperature and it will enable and enhance the separation and recovery

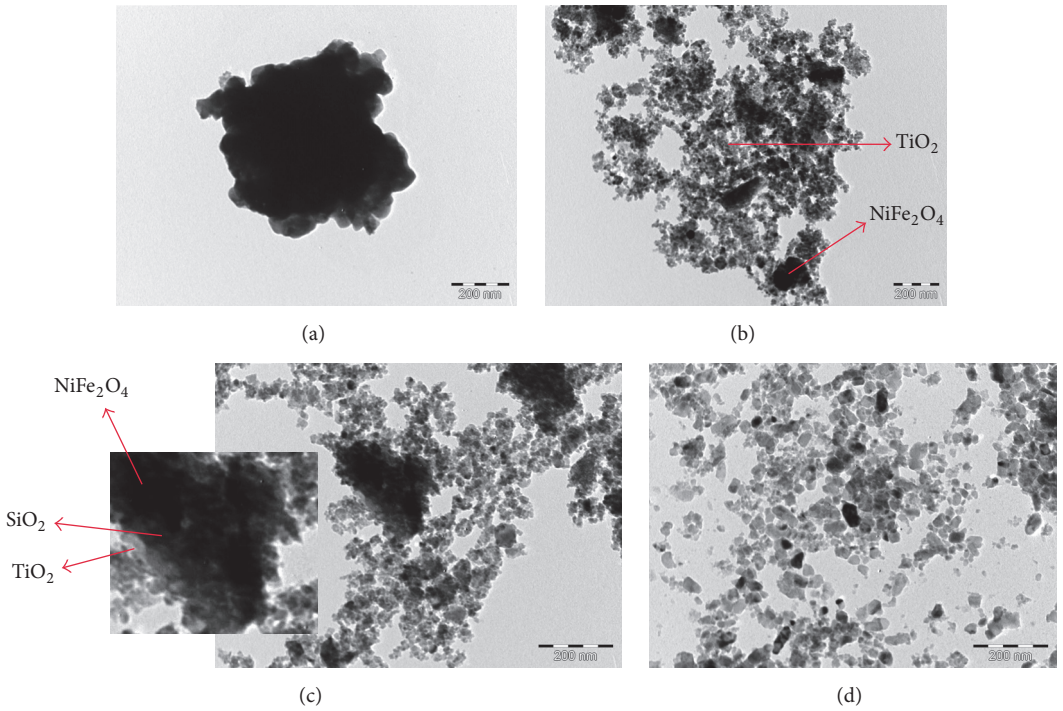

FIGURE 5: TEM micrographs of (a) $NiFe_2O_4$-SiO_2 nanoparticle, (b) $NiFe_2O_4$-TiO_2, (c) $NiFe_2O_4$-SiO_2-TiO_2, and (d) TiO_2 photocatalysts.

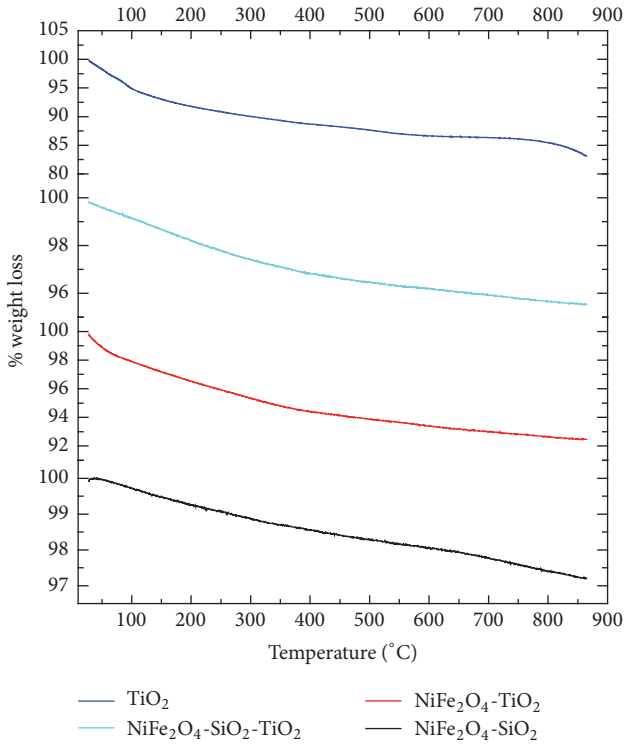

FIGURE 6: Thermograph of $NiFe_2O_4$-SiO_2 and photocatalysts.

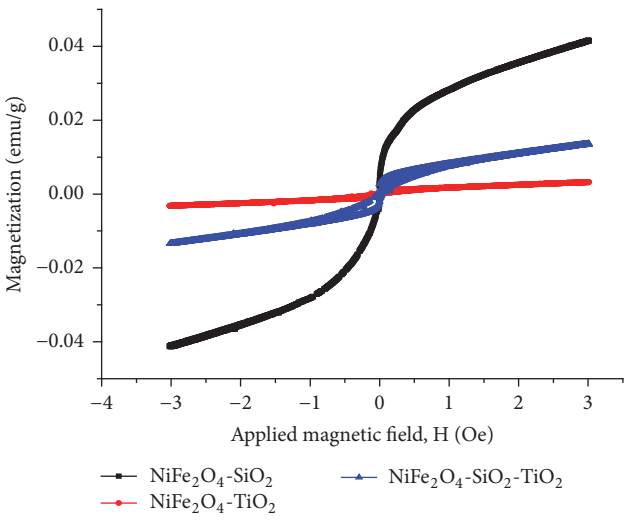

FIGURE 7: Magnetization hysteresis of $NiFe_2O_4$-SiO_2 and photocatalyst composites at 25°C.

of hybrid materials from aqueous solution using an external magnetic field.

3.2. Photocatalytic Experiment. The photocatalytic reduction of Cr(VI) by $NiFe_2O_4$-SiO_2, $NiFe_2O_4$-TiO_2, $NiFe_2O_4$-SiO_2-TiO_2, and TiO_2 was studied for its efficient reduction in contaminated wastewater. The reduction efficiencies of the photocatalysts were compared to determine the photocatalyst with the best capability to reduce Cr(VI). The effects of pH, time, and catalyst dose were studied to determine the optimum conditions for Cr(VI) reduction. Desorption studies were also studied for all the photocatalysts to ascertain the reusability of the photocatalysts.

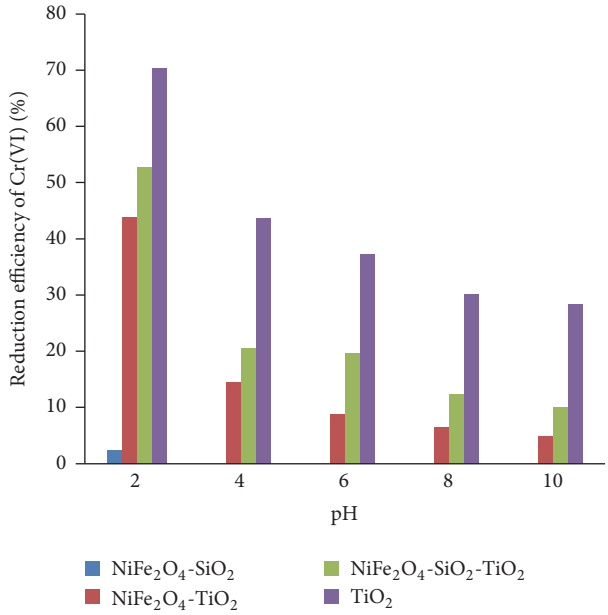

Figure 8: Effect of solution pH on the photocatalytic reduction of Cr(VI) (10 mg/L) for $NiFe_2O_4$-SiO_2 and photocatalysts at 20°C, 120 rpm for 1 h irradiation time under UV light.

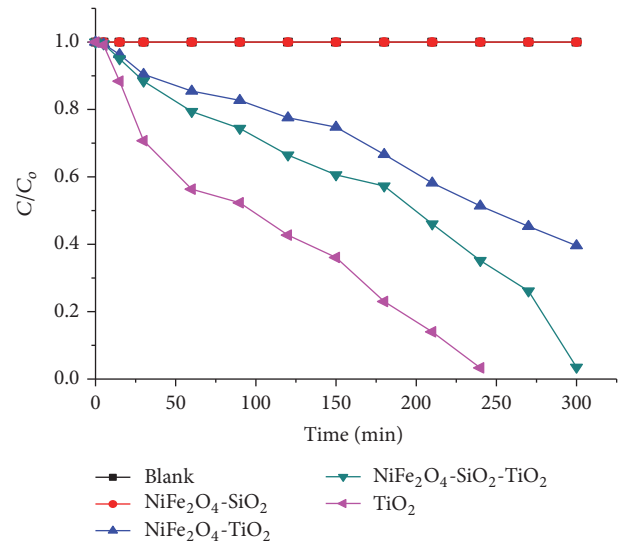

Figure 9: Effect of irradiation time on the photocatalytic reduction of Cr(VI) (10 mg/L) for blank, $NiFe_2O_4$-SiO_2, and photocatalyst materials at 20°C, pH 4, and 120 rpm and under UV light.

3.3. Effect of Solution pH. Solution pH in photocatalytic experiments is a vital factor to be considered as it can affect the surface charge of the photocatalyst. It has been reported that TiO_2 surface has three different species in water, $TiOH^+$, TiOH, and TiO^- [10]. At pH values higher than 5.5 (point of zero charge of TiO_2 photocatalyst), the surface of TiO_2 will have TiO^- species which repels Cr(VI) thereby affecting its adsorption on the surface of TiO_2 and with pH value less than 5.5 the surface will be positively charged and $Cr(OH)_3$ will be formed as a precipitate on the surface of TiO_2 which therefore aids the adsorption of Cr(VI) so that Cr(III) is deposited on the TiO_2 surface [33, 34]. Consequently, the effect of solution pH was carried out by exposing to UV light a known concentration of dichromate solution for 1 h with photocatalyst at room temperature. The solutions were adjusted to obtain an initial pH range of 2–10 using 0.1 mol dm^{-3} HCl or NaOH as the case may be. The effect of pH on the photocatalytic reduction of Cr(VI) using $NiFe_2O_4$-SiO_2, $NiFe_2O_4$-TiO_2, $NiFe_2O_4$-SiO_2-TiO_2, and TiO_2 under UV light is presented in Figure 8. The result showed that reduction efficiency of Cr(VI) increases as the solution pH decreases from 6 to 2 and reduces as the pH increases from 6 to 10 for $NiFe_2O_4$-TiO_2, $NiFe_2O_4$-SiO_2-TiO_2, and TiO_2 but for $NiFe_2O_4$-SiO_2 nanoparticle there was about 2% reduction of Cr(VI) at pH 10 and no photocatalytic reduction at all in the pH range lower than 10; this can be attributed to the fact that $NiFe_2O_4$-SiO_2 nanoparticles have little or no photocatalytic properties for the reduction of Cr(VI) in aqueous solution and that adsorption of Cr(VI) on its surface might have taken place. This trend is in agreement with previously published data [10, 35] on the reduction of Cr(VI) in aqueous solution indicating that in this study the process is determined by the adsorption of Cr(VI) on the surface of the photocatalysts and reduction efficiency is favoured in acidic solutions. Although the reduction of Cr(VI) was best in TiO_2 photocatalyst, for the composite samples, reduction efficiency was observed to be higher for $NiFe_2O_4$-SiO_2-TiO_2 than in $NiFe_2O_4$-TiO_2 at all pH levels (Figure 8); this could be attributed to the SiO_2interlayer present in the former. Similar result has been reported by Álvarez et al. [24]. All other photocatalytic reduction studies were conducted at a pH value of 4, since this value is within the reduction range for all the photocatalysts considered in this study.

3.4. Effect of Irradiation Time. In order to ascertain the irradiation time required to achieve maximum reduction, the photocatalytic reduction of Cr(VI) in aqueous solution using $NiFe_2O_4$-SiO_2, $NiFe_2O_4$-TiO_2, $NiFe_2O_4$-SiO_2-TiO_2, and TiO_2 photocatalyst was conducted for different time intervals. Figure 9 shows that photocatalytic reduction efficiency increases as the irradiation time increases for $NiFe_2O_4$-TiO_2, $NiFe_2O_4$-SiO_2-TiO_2, and TiO_2 photocatalysts while no reduction was observed for $NiFe_2O_4$-SiO_2. Also, Cr(VI) solution reached 96.5% photocatalytic reduction using $NiFe_2O_4$-SiO_2-TiO_2 within 300 min of UV irradiation compared to the 60% photocatalytic reduction using $NiFe_2O_4$-TiO_2 in 300 min. This higher photocatalytic reduction can be attributed to the SiO_2 interlayer covering and preventing the $NiFe_2O_4$ core from reducing the photocatalytic property of TiO_2 in the composite of $NiFe_2O_4$-SiO_2-TiO_2. This result is similar to the result obtained in a reported study [24]. This result reveals that the introduction of SiO_2 as an interlayer between magnetic titanium dioxide photocatalysts improved its photocatalytic properties and aids magnetic separation from aqueous solution. It is worthy of note that the best photocatalytic reduction was obtained within 240 min with TiO_2 photocatalyst (96.7% reduction

efficiency). $NiFe_2O_4$-SiO_2 and blank did not show any reduction in Cr(VI) after 300 min; this implies that $NiFe_2O_4$-SiO_2 and UV irradiation without photocatalyst cannot reduce Cr(VI) in aqueous solution.

3.5. Kinetic Study. The photoreduction of Cr(VI) in aqueous solution over different photocatalyst materials was plotted against irradiation time. Experimental data were fitted to the Langmuir-Hinshelwood (L-H) kinetic model:

$$r = \frac{-dc}{dt} = \frac{k_r\,(K)}{1} + KC, \tag{2}$$

where r is the rate of photoreduction (mg L^{-1} min^{-1}), C is the concentration of the reactant (mg L^{-1}), k is the equilibrium constant for the adsorption of Cr(VI) onto photocatalyst surface, t represents the equilibrium time, and K_r represents the specific reaction rate constant for the oxidation of the reactants (mg L^{-1} min^{-1}) [36]. Consequently, using pseudo-first-order kinetics, (2) can be simplified with an apparent first-order rate constant, K_{app}, and, by integrating it, (3) is obtained:

$$\ln \frac{C_o}{C} = \frac{K_r}{K_t} = K_{app}t, \tag{3}$$

where C_o represents the initial Cr(VI) concentration. When $\ln(C_o/C)$ is plotted against time (t), a straight line obtained indicates that the data obtained from the photocatalytic reduction of Cr(VI) using photocatalyst materials obeyed Langmuir-Hinshelwood (L-H) kinetic equation and the slope is the apparent first-order rate constant, K_{app}. Since R^2 helps to determine how exact the actual value is to the mean value, it can be observed in Figure 10 that a straight line was obtained from the data with R^2 values of 0.96136, 0.94901, and 0.97108 and corresponding K_{app} values of 0.00289 min^{-1}, 0.01049 min^{-1}, and 0.01371 min^{-1} for $NiFe_2O_4$-SiO_2, $NiFe_2O_4$-SiO_2-TiO_2, and TiO_2, respectively, indicating that all the data fitted well into the linear equation for the photocatalytic reduction of Cr(VI) solution conducted at pH 4.0 and 200 mg of $NiFe_2O_4$-SiO_2 and photocatalyst materials. The photocatalytic experiments successfully fitted well into the Langmuir-Hinshelwood (L-H) kinetic model and are described by the pseudo-first-order kinetics suggesting a surface reaction where Cr(VI) was absorbed at the rate determining step for the process. Similar results have been reported by Ku and Jung and Sun et al. [37, 38].

3.6. Effect of Catalyst Dose. The increasing effect of the amount of photocatalyst dose as a function of time on the reduction of Cr(VI) was studied by varying the amount of the photocatalysts ranging from 50 to 200 mg. Figure 11 illustrates the dependence of different photocatalysts composite dose on the photocatalytic reduction of Cr(VI) in aqueous solution under UV light. An increase in the reduction capacity of Cr(VI) was observed for all photocatalysts from 50 mg, 100 mg, 150 mg, and 200 mg catalyst dose (Figures 11(a), 11(b), 11(c), and 11(d)). Also, as the photocatalyst dose increases from 50 mg to 200 mg; the time for complete photocatalytic

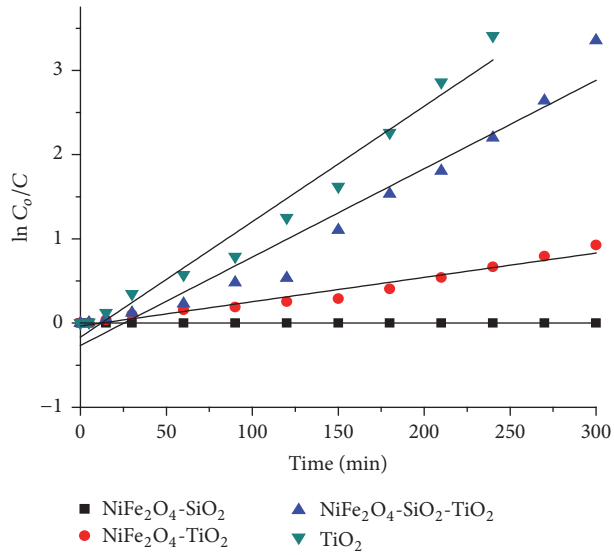

FIGURE 10: Linear plot of $\ln C_o/C$ against time (t) for the reduction of Cr(VI) using 200 mg of $NiFe_2O_4$-SiO_2 and photocatalysts.

reduction decreases; this is attributed to the fact that as the mass of photocatalyst is increased, the total number of active sites on the photocatalyst surface also increases thereby resulting in an increase in the amount of electrons which can be used for the photoreduction of Cr(VI). In increasing the photocatalyst dose beyond 200 mg, there exists a turbidity of the suspension which therefore reduces the penetration of light. Also, catalyst amount beyond 200 mg resulted in an aggregation; these cause a decrease in the number of active sites on the TiO_2 surface available for Cr(VI) reduction thereby resulting into a decrease in the performance of the photocatalysts [10].

However, $NiFe_2O_4$-SiO_2 did not reduce Cr(VI) in aqueous solutions for all photocatalyst dose confirming again its nonphotocatalytic capabilities towards Cr(VI) reduction in wastewater.

3.7. Regenerability and Reusability Study. For the use of the synthesized photocatalysts in the industry, it is important to test for the reusability potential of the spent photocatalysts for cost reduction and availability of photocatalysts for photocatalysis and environmental safety by limiting the disposal of secondary pollutants into the environment. In order to ascertain the reusability of these photocatalyst materials, 0.1 M NaOH was used to treat photocatalyst materials by agitating for 1 h. The choice of 0.1 M NaOH as the eluent for regeneration is attributed to the fact that the favourable pH for the reduction of Cr(VI) in aqueous solutions is the acidic pH range as earlier observed. Therefore, basic pH was not favourable for the adsorption of Cr(VI) on the photocatalysts surfaces and invariably weakens the force of adsorption under basic conditions. The results for the reuse of the photocatalyst materials for the reduction of Cr(VI) in 10 mg/L Cr(VI) solution after 3 cycles or runs are presented in Table 2. The result indicates that although the time for which the reduction of Cr(VI) occurred was slightly higher, the regenerated

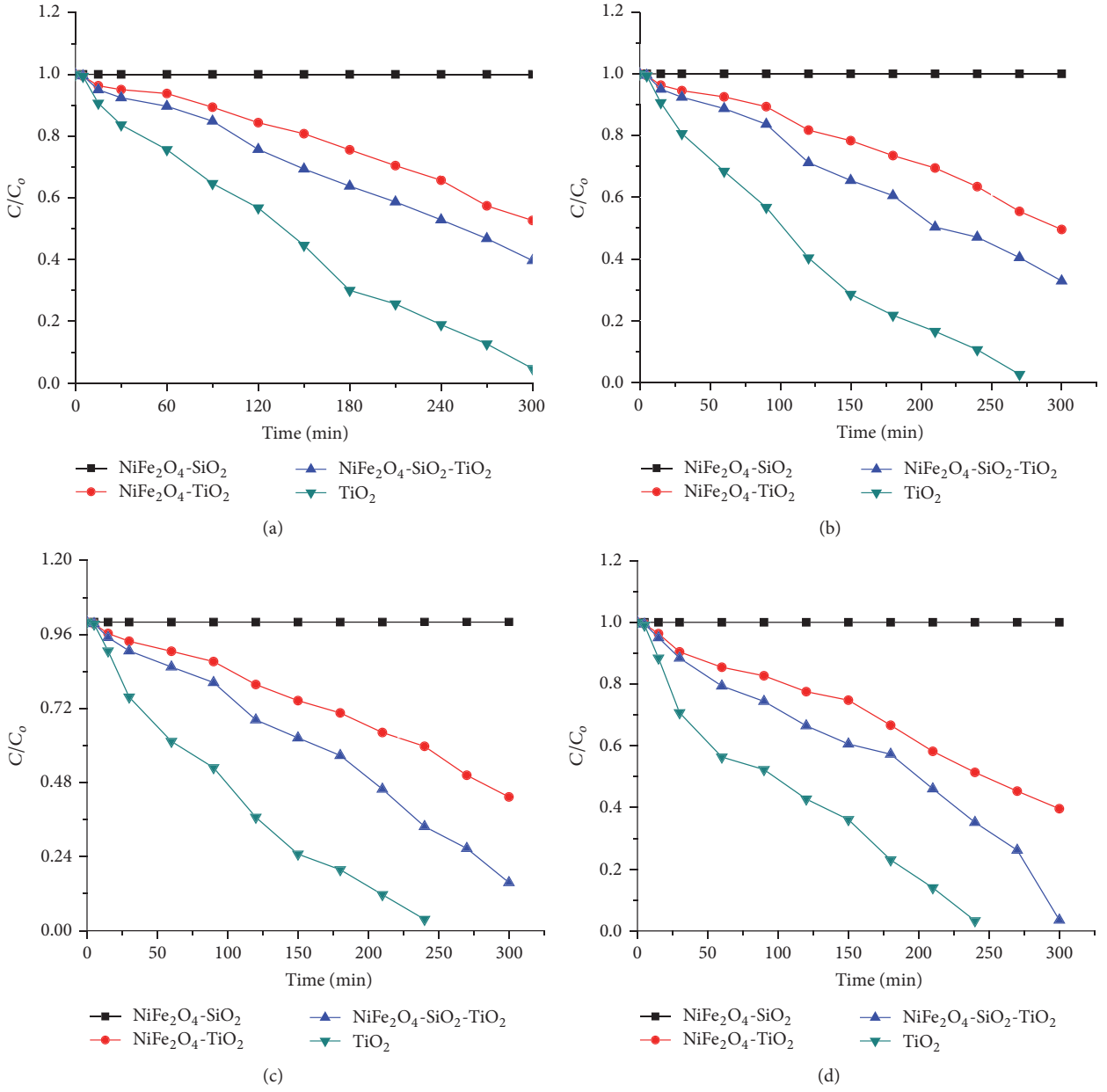

Figure 11: Effect of catalyst dose on the photocatalytic reduction of 100 cm^3 10 mg/L Cr(VI) at 120 rpm in the presence of (a) 50 mg, (b) 100 mg, (c) 150 mg, and (d) 200 mg of $NiFe_2O_4$-SiO_2 and photocatalysts under UV light at room temperature and 300 min irradiation time.

photocatalysts were still effective for the reduction of Cr(VI) in aqueous solution after 3 cycles or runs. TiO_2 showed better regenerability after 3 cycles or runs as it was able to reduce Cr(VI) completely after 270 min while $NiFe_2O_4$-SiO_2-TiO_2 had 68.92% reduction efficiency after 300 min and $NiFe_2O_4$-TiO_2 50.36% reduction efficiency. These results signify that the photocatalyst materials can be regenerated for reuse and that $NiFe_2O_4$-SiO_2-TiO_2 again performed better than $NiFe_2O_4$-TiO_2 showing better reusability. It is worth knowing that $NiFe_2O_4$-SiO_2 was not tested for its reusability in this study since it did not show any photocatalytic activity towards the reduction of Cr(VI) in aqueous solution.

4. Conclusion

The successful preparation of magnetic photocatalyst ($NiFe_2O_4$-SiO_2-TiO_2) by coating $NiFe_2O_4$, a magnetic core with a SiO_2 interlayer and hydrolyzing with photocatalytic TiO_2 was achieved. In addition, TiO_2 in an anatase phase, $NiFe_2O_4$-TiO_2, and $NiFe_2O_4$-SiO_2 were also synthesized for the reduction of Cr(VI) in aqueous solution. FTIR and XRD analysis confirmed the formation and coexistence of anatase TiO_2 and spinel $NiFe_2O_4$ while microscopic studies revealed that TiO_2 photocatalyst was deposited on ferrite nanoparticle in the composites. Photocatalytic

Table 2: Reusability study showing the % reduction efficiency of Cr(VI) after 3 runs using 200 mg photocatalyst at pH 4 for 300 min.

Time (min)	1st run (%)			2nd run (%)			3rd run (%)		
	NT	NST	TiO_2	NT	NST	TiO_2	NT	NST	TiO_2
0	0	0	0	0	0	0	0	0	0
5	0.497	0.551	0.92	0.408	0.503	0.844	0.259	0.294	0.621
15	3.683	4.974	11.60	2.961	4.426	10.248	2.004	3.636	8.33
30	9.576	11.602	29.28	8.491	10.816	28.661	6.219	7.56	19.509
60	14.512	20.626	43.64	13.62	19.534	42.963	9.531	10.86	30.621
90	17.311	38.31	54.69	16.011	24.525	50.215	12.538	14.229	44.335
120	22.449	41.44	71.27	21.966	38.661	62.55	18.88	19.48	56.804
150	25.23	66.85	80.29	24.606	51.599	75.53	20.795	26.585	68.5
180	33.333	78.45	89.50	31.961	66.231	82.08	26.216	33.551	76.13
210	41.768	83.61	94.29	40.31	72.741	89.09	32.706	48.606	82.61
240	48.674	88.95	96.69	48.001	79.495	94.77	36.592	56.07	90.0
270	54.788	92.82	100	53.662	85.536	100	44.68	61.254	100
300	60.424	96.50	100	59.311	90.08	100	50.361	68.92	100

Key. NT: nickel titanium dioxide photocatalyst; NST: nickel silane titanium dioxide photocatalyst.

experiments show that $NiFe_2O_4$-SiO_2-TiO_2 has higher reduction efficiency than magnetic titanium dioxide without silica interlayer ($NiFe_2O_4$-TiO_2). TiO_2 was observed to be the best photocatalyst for the reduction of Cr(VI) in a simulated wastewater sample with 96.7% reduction efficiency within 240 min while $NiFe_2O_4$-SiO_2-TiO_2 has 96.5% reduction efficiency within 300 min and $NiFe_2O_4$-TiO_2 gave 60% reduction efficiency within 300 min of UV irradiation. This study demonstrates that incorporating silica layer between magnetic core and photocatalyst such as titanium dioxide can significantly improve and enhance the photocatalytic properties without affecting the magnetic recovery of magnetic titanium dioxide nanocomposites in aqueous solutions, therefore making them suitable photocatalysts for wastewater decontamination.

As the pH reduces, the reduction efficiency of all photocatalysts for Cr(VI) in wastewater increases. Also, increase in the photocatalyst dose increases the reduction capacity towards Cr(VI) in aqueous solution. Kinetic study shows that reduction of Cr(VI) by photocatalyst materials took place at the surface of the materials obeying Langmuir-Hinshelwood (L-H) kinetic model and described by the pseudo-first-order kinetics. The regeneration of photocatalyst materials was successful, suggesting that reusability of the spent materials for the reduction of secondary pollutants is possible. Thus, the synthesized photocatalyst material ($NiFe_2O_4$-SiO_2-TiO_2) showed great and enhanced capabilities for the removal of contaminants from the environment through photocatalysis.

Competing Interests

The authors wish to declare that there is no conflict of interests regarding the publication of this manuscript.

Acknowledgments

The authors are grateful to the South Africa Medical Research Council for financial support.

References

[1] F. Fu and Q. Wang, "Removal of heavy metal ions from wastewaters: a review," *Journal of Environmental Management*, vol. 92, no. 3, pp. 407–418, 2011.

[2] J. J. Testa, M. A. Grela, and M. I. Litter, "Heterogeneous photocatalytic reduction of chromium(VI) over TiO_2 particles in the presence of oxalate: involvement of Cr(V) species," *Environmental Science & Technology*, vol. 38, no. 5, pp. 1589–1594, 2004.

[3] J. D. Willey and S. D. Zvalaren, "Chromium speciation in rainwater: temporal variability and atmospheric deposition," *Environmental Science & Technology*, vol. 36, no. 24, pp. 5321–5327, 2002.

[4] S. Chakrabarti, B. Chaudhuri, S. Bhattacharjee, A. K. Ray, and B. K. Dutta, "Photo-reduction of hexavalent chromium in aqueous solution in the presence of zinc oxide as semiconductor catalyst," *Chemical Engineering Journal*, vol. 153, no. 1–3, pp. 86–93, 2009.

[5] A. Y. Zahrim and N. Hilal, "Treatment of highly concentrated dye solution by coagulation/flocculation-sand filtration and nanofiltration," *Water Resources and Industry*, vol. 3, pp. 23–34, 2013.

[6] A. L. Ahmad, W. A. Harris, Syafiie, and B. S. Ooi, "Removal of dye from wastewater of textile industry using membrane technology," *Jurnal Teknologi*, vol. 36, 2002.

[7] Y. Ma, J.-B. Qiu, Y.-A. Cao, Z.-S. Guan, and J.-N. Yao, "Photocatalytic activity of TiO_2 films grown on different substrates," *Chemosphere*, vol. 44, no. 5, pp. 1087–1092, 2001.

[8] S. B. Jonnalagadda and S. Nadupalli, "Effluent treatment using electrochemically bleached seawater—oxidative degradation of pollutants," *Talanta*, vol. 64, no. 1, pp. 18–22, 2004.

[9] T. Robinson, G. McMullan, R. Marchant, and P. Nigam, "Remediation of dyes in textile effluent: a critical review on current treatment technologies with a proposed alternative," *Bioresource Technology*, vol. 77, no. 3, pp. 247–255, 2001.

[10] Y. A. Shaban, "Effective photocatalytic reduction of Cr(VI) by carbon modified (CM)-n-TiO_2 nanoparticles under solar irradiation," *World Journal of Nano Science and Engineering*, vol. 03, no. 04, pp. 154–160, 2013.

[11] Y. He, Y. Wang, L. Zhang, B. Teng, and M. Fan, "High-efficiency conversion of CO_2 to fuel over ZnO/g-C_3N_4 photocatalyst," *Applied Catalysis B: Environmental*, vol. 168-169, pp. 1–8, 2015.

[12] Y. Wang, Q. Lai, F. Zhang et al., "High efficiency photocatalytic conversion of CO_2 with H_2O over Pt/TiO_2 nanoparticles," *RSC Advances*, vol. 4, no. 84, pp. 44442–44451, 2014.

[13] L. Luo, A. T. Cooper, and M. Fan, "Preparation and application of nanoglued binary titania-silica aerogel," *Journal of Hazardous Materials*, vol. 161, no. 1, pp. 175–182, 2009.

[14] H. Yao, M. Fan, Y. Wang, G. Luo, and W. Fei, "Magnetic titanium dioxide based nanomaterials: synthesis, characteristics, and photocatalytic application in pollutant degradation," *Journal of Materials Chemistry A: Materials for Energy and Sustainability*, vol. 3, no. 34, pp. 17511–17524, 2015.

[15] S. Yamazaki, S. Matsunaga, and K. Hori, "Photocatalytic degradation of trichloroethylene in water using TiO_2 pellets," *Water Research*, vol. 35, no. 4, pp. 1022–1028, 2001.

[16] I. M. Arabatzis, S. Antonaraki, T. Stergiopoulos et al., "Preparation, characterization and photocatalytic activity of nanocrystalline thin film TiO_2 catalysts towards 3,5-dichlorophenol degradation," *Journal of Photochemistry and Photobiology A: Chemistry*, vol. 149, no. 1–3, pp. 237–245, 2002.

[17] A. Y. Shan, T. I. M. Ghazi, and S. A. Rashid, "Immobilisation of titanium dioxide onto supporting materials in heterogeneous photocatalysis: a review," *Applied Catalysis A: General*, vol. 389, no. 1-2, pp. 1–8, 2010.

[18] Y. Gao, B. Chen, H. Li, and Y. Ma, "Preparation and characterization of a magnetically separated photocatalyst and its catalytic properties," *Materials Chemistry and Physics*, vol. 80, no. 1, pp. 348–355, 2003.

[19] Y. S. Chung, S. B. Park, and D.-W. Kang, "Magnetically separable titania-coated nickel ferrite photocatalyst," *Materials Chemistry and Physics*, vol. 86, no. 2-3, pp. 375–381, 2004.

[20] T.-L. Su, C.-S. Chiou, and H.-W. Chen, "Preparation, photocatalytic activity, and recovery of magnetic photocatalyst for decomposition of benzoic acid," *International Journal of Photoenergy*, vol. 2012, Article ID 909678, 8 pages, 2012.

[21] J. Jing, J. Li, J. Feng, W. Li, and W. W. Yu, "Photodegradation of quinoline in water over magnetically separable Fe_3O_4/TiO_2composite photocatalysts," *Chemical Engineering Journal*, vol. 219, pp. 355–360, 2013.

[22] K. Maaz, A. Mumtaz, S. K. Hasanain, and A. Ceylan, "Synthesis and magnetic properties of cobalt ferrite ($CoFe_2O_4$) nanoparticles prepared by wet chemical route," *Journal of Magnetism and Magnetic Materials*, vol. 308, no. 2, pp. 289–295, 2007.

[23] K. Laohhasurayotin, S. Pookboonmee, D. Viboonratanasri, and W. Kangwansupamonkon, "Preparation of magnetic photocatalyst nanoparticles—TiO_2/SiO_2/Mn–Zn ferrite—and its photocatalytic activity influenced by silica interlayer," *Materials Research Bulletin*, vol. 47, no. 6, pp. 1500–1507, 2012.

[24] P. M. Álvarez, J. Jaramillo, F. López-Piñero, and P. K. Plucinski, "Preparation and characterization of magnetic TiO2 nanoparticles and their utilization for the degradation of emerging pollutants in water," *Applied Catalysis B: Environmental*, vol. 100, no. 1-2, pp. 338–345, 2010.

[25] Y. Li, M. Zhang, M. Guo, and X. Wang, "Preparation and properties of a nano TiO_2/Fe_3O_4 composite superparamagnetic photocatalyst," *Rare Metals*, vol. 28, no. 5, pp. 423–427, 2009.

[26] H. Hamad, M. Abd El-Latif, A. E.-H. Kashyout, W. Sadik, and M. Feteha, "Synthesis and characterization of core–shell–shell magnetic ($CoFe_2O_4$–SiO_2–TiO_2) nanocomposites and TiO_2 nanoparticles for the evaluation of photocatalytic activity under UV and visible irradiation," *New Journal of Chemistry*, vol. 39, no. 4, pp. 3116–3128, 2015.

[27] R. Li, Y. Jia, J. Wu, and Q. Zhen, "Photocatalytic degradation and pathway of oxytetracyclin in aqueous solution by Fe_3O_4–TiO_2 nanopowder," *RSC Advances*, vol. 5, no. 51, pp. 40764–40771, 2015.

[28] X. Huang and Z. Chen, "Preparation of $CoFe_2O_4$/SiO_2 nanocomposites by sol-gel method," *Journal of Crystal Growth*, vol. 271, no. 1-2, pp. 287–293, 2004.

[29] S. Yang, Y. Guo, X. Zhou, C. Lin, Y. Wang, and W. Zhang, "Enhanced photocatalytic activity for degradation of methyl orange over silica-titania," *Journal of Nanomaterials*, vol. 2011, Article ID 296953, 9 pages, 2011.

[30] H. G. Yang and H. C. Zeng, "Preparation of hollow anatase TiO_2 nanospheres via Ostwald ripening," *Journal of Physical Chemistry B*, vol. 108, no. 11, pp. 3492–3495, 2004.

[31] W. Wu, X. Xiao, S. Zhang, F. Ren, and C. Jiang, "Facile method to synthesize magnetic iron oxides/TiO_2 hybrid nanoparticles and their photodegradation application of methylene blue," *Nanoscale Research Letters*, vol. 6, article 533, pp. 1–15, 2011.

[32] B. Palanisamy, C. M. Babu, B. Sundaravel, S. Anandan, and V. Murugesan, "Sol–gel synthesis of mesoporous mixed Fe_2O_3/TiO_2 photocatalyst: application for degradation of 4-chlorophenol," *Journal of Hazardous Materials*, vol. 252-253, pp. 233–242, 2013.

[33] N. Wang, Z. Chen, L. Zhu, X. Jiang, B. Lv, and H. Tang, "Synergistic effects of cupric and fluoride ions on photocatalytic degradation of phenol," *Journal of Photochemistry and Photobiology A: Chemistry*, vol. 191, no. 2-3, pp. 193–200, 2007.

[34] C. Shifu and C. Gengyu, "Study on the photocatalytic reduction of dichromate and photocatalytic oxidation of dichlorvos," *Chemosphere*, vol. 60, no. 9, pp. 1308–1315, 2005.

[35] C. M. Ma, Y. S. Shen, and P. H. Lin, "Photoreduction of Cr(VI) ions in aqueous solutions by UV/TiO_2 photocatalytic processes," *International Journal of Photoenergy*, vol. 2012, Article ID 381971, 7 pages, 2012.

[36] X. Lou, J. Han, W. Chu, X. Wang, and Q. Cheng, "Synthesis and photocatalytic property of Co_3O_4 nanorods," *Materials Science and Engineering B*, vol. 137, no. 1–3, pp. 268–271, 2007.

[37] Y. Ku and I.-L. Jung, "Photocatalytic reduction of Cr(VI) in aqueous solutions by UV irradiation with the presence of titanium dioxide," *Water Research*, vol. 35, no. 1, pp. 135–142, 2001.

[38] J. Sun, X. Wang, J. Sun, R. Sun, S. Sun, and L. Qiao, "Photocatalytic degradation and kinetics of Orange G using nano-sized Sn(IV)/TiO_2/AC photocatalyst," *Journal of Molecular Catalysis A: Chemical*, vol. 260, no. 1-2, pp. 241–246, 2006.